A&A 586, A58 (2016)
DOI: 10.1051/0004-6361/201527239
© ESO 2016

Astronomy & Astrophysics

Multi-colour optical photometry of V404 Cygni in outburst *(Research Note)*

Josep Martí[1], Pedro L. Luque-Escamilla[2], and María T. García-Hernández[1]

[1] Departamento de Física, Escuela Politécnica Superior de Jaén, Universidad de Jaén, Campus Las Lagunillas s/n, A3, 23071 Jaén, Spain
e-mail: [jmarti;tgarcia]@ujaen.es
[2] Departamento de Ingeniería Mecánica y Minera, Escuela Politécnica Superior de Jaén, Universidad de Jaén, Campus Las Lagunillas s/n, A3, 23071 Jaén, Spain
e-mail: peter@ujaen.es

Received 24 August 2015 / Accepted 21 December 2015

ABSTRACT

Context. This observational paper has been prepared in the context of the large multi-wavelength effort by many observers with the aim of following up the transient flaring event of V404 Cygni that took place for several weeks in 2015 June.
Aims. Our main original aim was to contribute to the study of this transient source by acquiring broad-band photometric observations during its most active flaring phases. Nevertheless, after a detailed analysis of the data, several interesting results were obtained that encouraged a dedicated publication.
Methods. The methodology used was based on broad-band differential CCD photometry. This outburst of V404 Cygni rendered the source a very bright target easily within reach of small educational telescopes. Therefore, the 41 cm telescope available at the Astronomical Observatory of the University of Jaén was used in this work.
Results. We detected variability at different time scales, both in amplitude and colour. Individual optical flares appear every half hour on average during our 3 h long observation, although large-amplitude (∼1 mag) variations are also observed to occur on intervals as short as 10 min. Also, colour variations appear to be highly correlated in a colour-colour diagram. Another remarkable finding is the detection of time lag, from about one to a fraction of a minute between light curves in different filters (VR_cI_c).
Conclusions. The observed behaviour is tentatively interpreted in an scenario based on the ejection of non-thermal emitting, relativistic plasmons, with their synchrotron spectra extending up to optical wavelengths. This would render some of the V404 Cygni flares very similar to those of the well-know microquasar GRS 1915+105

Key words. X-rays: binaries – stars: jets – stars: individual: V404 Cygni

1. Introduction

V404 Cygni also known as GS 2023+338 is a low-mass X-ray binary (LMXB) originally discovered during its 1989 outburst by the Japanese GINGA satellite (Kitamoto et al. 1989). Intensive photometric and spectroscopic follow-up of this historical event yielded an orbital period of about 6.5 d and remarkably concluded with the presence of a massive stellar black hole in the system (Casares et al. 1992; Wagner et al. 1992). The companion star of V404 Cygni has been proposed to be an object of a late-type K0(±1) III-V spectral type (Casares et al. 1993). Radio detections using Very Long Baseline Interferometry (VLBI) enabled an accurate parallax measurement that places V404 Cygni at a distance of 2.39 ± 0.14 kpc (Miller-Jones et al. 2009). These VLBI observations also constrained the size of any quiescent jets to less than 1.4 AU. The quiescent X-ray spectrum has a power-law photon index $\Gamma \simeq 2.0$ seen through a a total column density of $N_{\rm H} = (1.0 \pm 0.1) \times 10^{22}$ cm^{-2} (see e.g. Reynolds et al. 2014, and references therein). The unabsorbed 0.3–10 keV luminosity approaches several times 10^{32} erg s^{-1}, thus making V404 Cygni the brightest black hole LMXB in quiescence.

On 16 June 2015, V404 Cygni was reported to be in outburst by the *Swift* Burst Alert Telescope (Barthelmy et al. 2015), and soon confirmed by the Monitor of All-sky X-ray Image on board the International Space Station (Negoro et al. 2015). After these early warnings, an intensive observational effort was deployed by many observers that was quickly reflected in an intense flow of tens of related electronic telegrams. Soon, it became evident that this was an extraordinary outburst event after decades of quiescence. Optical, infrared, radio, X-ray and gamma-ray telescopes have so far collected an impressive amount of data that will emerge in the scientific literature in the upcoming months. But the extraordinary thing was that even small optical telescopes could join this endeavor since V404 Cygni became a bright and highly variable source at visible wavelengths (Hynes et al. 2015; Hardy et al. 2015; Wiersema 2015; Scarpaci & Maitra 2015).

In this work, we present the optical data acquired using the educational astronomical facilities available at the University of Jaén (UJA). Our aim is to contribute to the wealth of public astronomical data about this transient event while, at the same time, attempting to better constrain the nature of this phenomenon.

2. Observations

The observations were carried out on 26 June 2015 from the UJA Astronomical Observatory. The observatory is located in an urban area inside the Campus of Las Lagunillas, and hosts an automated 41 cm Schmidt-Cassgrain with f/8 focal ratio. The UJA telescope, heareafter UJT, operates using a ST10-XME commercial CCD camera with 2184 × 1472 pixels of 6.8 μm size. The pixel scale is 0.″42 pixel^{-1}. The camera is equipped with a wheel of $UBVR_cI_c$ Johnson-Cousins filters (Johnson & Morgan 1953; Cousins 1974a,b) manufactured according to the Bessell filter prescription (Bessell 1979). The seeing average was typically of about 2″, and therefore 2 × 2 binning was used.

Differential VR_cI_c photometry was performed on V404 Cygni during 3 h with exposure times of 60 s in each filter. The total number of measurements acquired per filter was N_{obs} = 51. Four comparison stars in the field were used whose photometric behaviour, within 0.01–0.02 mag, was found to be very stable in all bands. Their VR_cI_c magnitudes were retrieved from the AAVSO database[1], and are given in Table A.1. Photometry in U and B-bands was not acquired because of very low source counts. For each observed photometric band, here generically indicated by an effective wavelength λ, the magnitudes of the variable target m_λ^{var} were derived with respect to the comparison stars according to:

$$m_\lambda^{var} = m_\lambda^{com} + \Delta m_{\lambda,ins} + T_{\lambda,C_\lambda}\Delta C_{\lambda,ins}, \quad (1)$$

where m_λ^{com} is the magnitude of the comparison star being used, and $\Delta m_{\lambda,ins}$ and $\Delta C_{\lambda,ins}$ are the instrumental differences in magnitude and colour between the target and comparison star, respectively. The factor T_{λ,C_λ} is the colour transformation coefficient that was separately determined using standards in clusters and other fields. The colour $(V - R_c)$ was used in Eq. (1) for V- and R_c-band observations, while the colour $(V - I_c)$ was preferred for I_c-band observations instead. The system photometric properties are approximately stable from night to night and we typically obtain $|T_{\lambda,C_\lambda}| < 0.1$. Finally, the different measurements of m_λ^{var} were weighted according to their respective uncertainty and then averaged. The corresponding results are presented in Table A.2 and Figs. 1 and 2. The errors quoted here are representative of the differential photometry process, and do not include the uncertainty in the absolute calibration of the comparison stars (~0.02 mag). Main flaring events in Fig. 1 are labelled from 1 to 6 for later discussion.

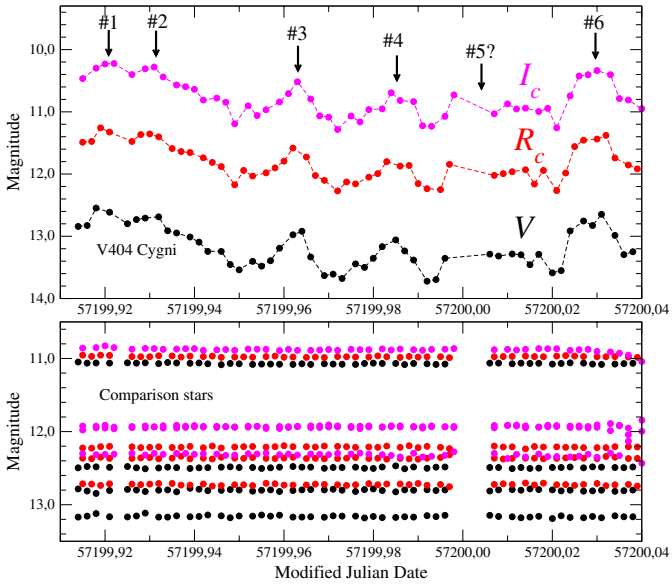

Fig. 1. *Top*: light curves of V404 Cygni in outburst as observed with the UJT on 26 June 2015 in the V, R and I-bands. Flares are labelled for clarity using vertical arrows. *Bottom*: behaviour of the four comparison stars, plotted at the same scale, which remained constant in brightness within 0.01–0.02 mag.

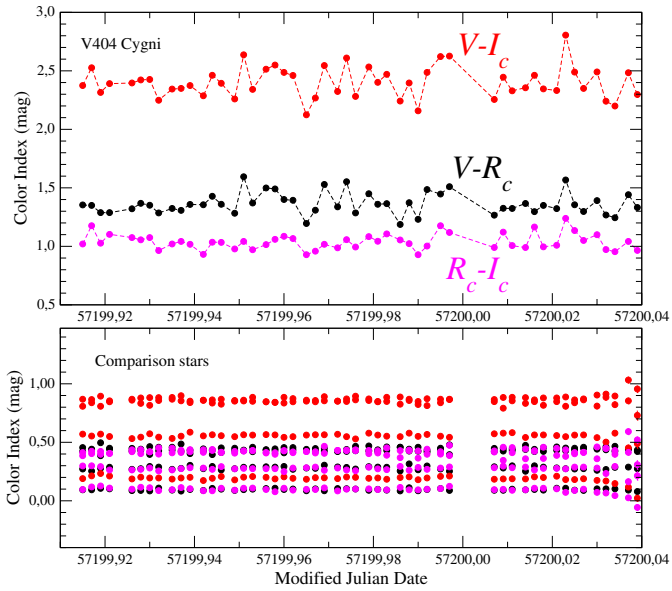

Fig. 2. *Top*: variability of colour indices $V - R$, $V - I$ and $R - I$ of V404 Cygni in outburst as observed with the UJT on 26 June 2015. They are shown plotted in black, red, and magenta colours, respectively. *Bottom*: the same kind of plot for the four comparison stars plotted at the same scale. Their colours remained constant within 0.02–0.03 mag.

3. Discussion

The light curves in Figs. 1 and 2 clearly show how V404 Cygni varied and flared intensively during the observation. The amplitude of variation was as large as one magnitude and several tenths of a magnitude in brightness and colour, respectively. These variations occurred on timescales as short as 10 min. The significance and intrinsic origin of these flares is ensured given that the comparison stars remained practically flat within a few hundreds of a magnitude. This agrees well with the behaviour reported by different observers at other times during the intensive coverage of the outburst (e.g. Hynes et al. 2015). From causality arguments, our data puts a coarse upper limit of ~1 AU to the region from where the optical emission arises in the vicinity of the accretion disk around the V404 Cygni black hole.

It is also very interesting that the observed variability apparently followed a clear pattern in colour–colour diagrams. This is illustrated in Fig. 3 where the pattern becomes more evident as the source evolved in a very restricted region of the diagram. A simple regression fit yields a correlation coefficient as high as 0.89, thus suggesting that a strong connection between the source colours existed during the flaring events. The modelling

[1] American Association of Variable Stars Observers, http://www.aavso.org and references therein.

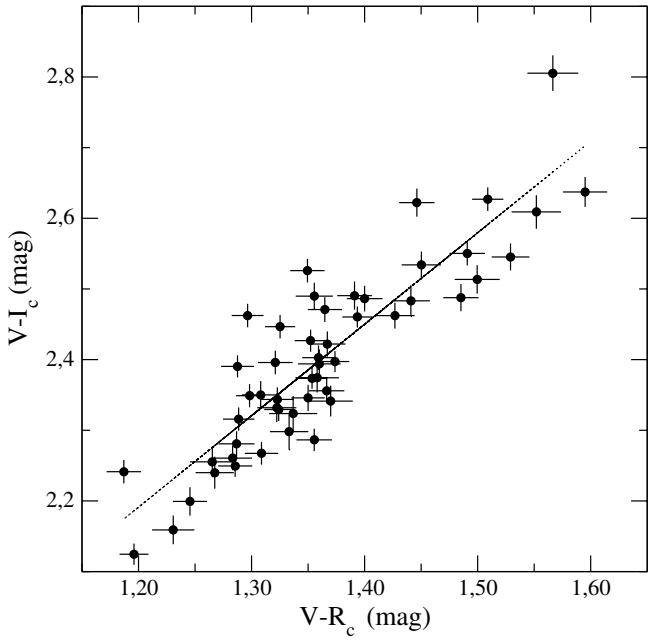

Fig. 3. Evolution of V404 Cygni in the colour–colour plane during a few hours on 26 June 2015 as observer with the UJT. The dotted line is a linear regression fit guiding the eye to better appreciate the colour–colour correlation suggested in the text.

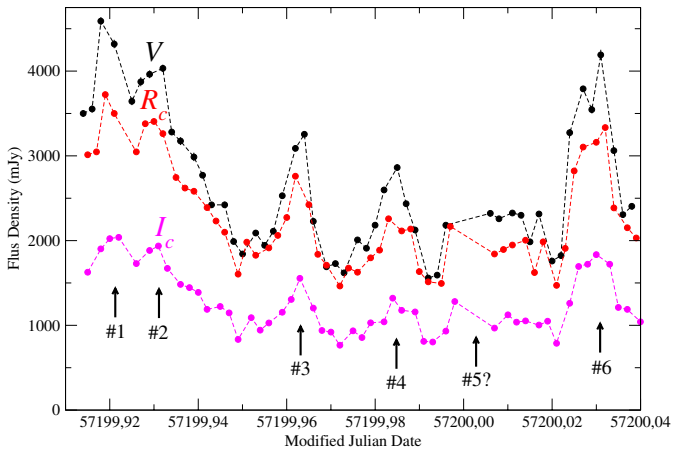

Fig. 4. Dereddened light curves of V404 Cygni in outburst as observed with the UJT on 26 June 2015 in the V, R_c and I_c-bands assuming an interstellar extinction of $A_V = 4.0$ mag. The brightness level has been converted from magnitudes to a flux density scale, in mJy units. Flares are labelled as in Fig. 1.

of such behaviour is beyond the observational scope of this paper, and we limit ourselves here to state this observational fact. Nevertheless, we speculate that it could be intimately linked to the source spectral evolution discussed below.

The intrinsic amplitudes of the observed flares become more obvious when de-reddening the photometric observations, and expressing them in terms of flux density. The interstellar extinction law in Mathis (2000) was used for de-reddening purposes. This is presented in Fig. 4, where two isolated flares (#3 and #4) are easily visible with their peaks separated by nearly a half hour. Other flaring events both at the beginning (#1 and #2) and the end (#5 and #6) of the observation are also present within comparable time intervals. However, their individual evolution cannot be so easily disentangled because they are close in time or not well sampled. By analogy with other similar flaring behaviours, such as in the LMXB GRS 1915+105 at radio and near-infrared wavelengths (Mirabel et al. 1998), one is tempted to interpret this recursive flare pattern as episodes of replenishment and emptying of the inner accretion disk. These kind of events come accompanied by the ejection of plasmons along collimated jets as a result of accretion disk instabilities. These plasma clouds typically have a characteristic non-thermal, synchrotron emission mechanism. Their spectrum spans from radio to much shorter wavelengths depending on the energy cut-off of relativistic electrons and the strength of magnetic field. The fact that strong radio emission from V404 Cygni was detected in 1.4 GHz observations carried out just six hours before ours, peaking at 0.364 ± 0.030 Jy (Tsubono et al. 2015), would be naturally understood in this context. The similarity between V404 Cygni and GRS 1915+105 has already been noted by Mooley et al. (2015).

The observed optical flares appeared superimposed onto an average pedestal emission level likely due to hot accretion disk in V404 Cygni. From Fig. 4, the average de-reddened flux densities were found to be 2.27 ± 0.16, 2.02 ± 0.11, and 1.10 ± 0.04 Jy in the V, R_c and I_c-bands, respectively. By fitting a simple power law, the average spectral energy distribution (SED) of V404 Cygni depends on frequency roughly as $\propto \nu^{2.1\pm0.3}$. No correction for the contribution of the Hα emission line to R_c-band data has been attempted here. The resulting power law index is consistent with the UJT data sampling the Raleigh Jeans ν^2 part of the accretion disk spectrum. Extrapolation of this power law to the radio band falls orders of magnitude below the reported radio flux densities. Therefore, an additional emission component must exist to explain the Tsubono et al. (2015) radio detection. As stated before, this component is most naturally interpreted as originating in plasma ejection events.

In the scenario outlined here, one would expect the peak time of an individual flare to be dependent on the wavelength of observation. According to the simple van der Laan (1966) model of a synchrotron-emitting expanding plasmon, the light curve observed at a wavelength λ reaches its maximum after a time given by

$$t_{m,\lambda} = t_{m,\lambda_0}[\lambda/\lambda_0]^{-\frac{p+4}{4p+6}}, \quad (2)$$

where t_{m,λ_0} is the time of maximum at a reference wavelength λ_0, and p is the power-law index of the energy distribution of relativistic electrons.

In the absence of contemporaneous high time resolution radio photometry, where a λ-dependent delay would be easier to measure, we searched our optical data for possible time lags between the different light curves at V, R_c and I_c-bands. Taking, for instance, the isolated flare #3, which peaks around MJD 57 199.965 in Figs. 1 and 4, the rising time from the pedestal emission level to the flare peak in the V-band is $t_{m,V} \simeq 0.01$ d. Assuming $p \simeq 1.0$, and given that the central effective wavelengths of our photometric filer set ($\lambda_V = 0.545$ μm, $\lambda_{R_c} = 0.641$ μm, and $\lambda_{I_c} = 0.798$ μm), we can estimate the expected time delays in the UJT observations. Using Eq. (2), and taking the V-band as reference, the predicted delays are 1.2 min and 3.0 min for the R_c and I_c-band, respectively. Similarly, a 1.8 min delay would be expected between I_c and R_c data. Assuming other reasonable values of p does not change significantly these numbers. For instance, taking $p = 2.5$ one gets delays of 1.0 min, 2.4 min, and 1.4 min, respectively.

What happens with real data? To answer this question, we performed a cross-correlation function (CCF) exercise between

the different UJT light curves. A problem arises here because the data are not evenly spaced in time. The CCF calculation was then carried out in two different ways. The first calculation was specially designed for such irregular time series and is based on averaging data products with similar time lags within a user defined binning (Edelson & Krolik 1988). The second calculation simply makes a linear interpolation to obtain a regular sampling of the data from which the traditional estimator of the CCF is computed. In our case, this second approach is justified because our observations were nearly evenly spaced. When applying the first method, the resulting CCFs do not have enough resolution to clearly establish a non-zero time lag although hints of delay between the longer and shorter wavelength filters were obtained. In contrast, the interpolation method provided well-defined CCF maxima shifted from zero (Figs. A.1 and A.2). Here, the key fact is that all maxima occur with a clearly negative lag, i.e. consistent with the longer wavelength light curves that are delayed with respect to the shorter wavelength curves, as expected. Interestingly, similar negative time lags have also been observed in some of the V404 Cygni flares seen by the INTEGRAL satellite (Rodriguez et al. 2015), where the optical V-band emission was delayed with respect to hard X-rays and soft γ-rays from 1.5 to 20–30 min. However, these lags correspond to extremely different energy bands in contrast to our results here reported within the optical domain.

The measured offset of the maxima with respect to the origin (in Figs. A.1 and A.2) indicates that the I_c-band light curve is delayed with respect to V-band by 108 ± 1 s, while the R_c-band lags it by 34 ± 1 s. Concerning the two reddest filters, I_c-band also lags the R_c-band by 34 ± 1 s. The uncertainties in the estimates of the CCF peak positions were derived using the White & Peterson (1994) formula

$$\Delta\tau = \frac{0.38 W_{\rm CCF}}{1 + r_{\rm max}(N_{\rm total} - 2)^{1/2}}, \tag{3}$$

where $W_{\rm CCF}$ is the full width at half maximum of the CCF peak with $r_{\rm max}$ amplitude, and $N_{\rm total} = (N_{\rm obs} - 1)N$ the full number of available points, where N is the amount of sampling points. In our case, $W_{\rm CCF} \simeq 1000$ s, $r_{\rm max} \simeq 1$, and we interpolated up to $N = 10^4$ points.

Although these numbers are not identical to the values anticipated using Eq. (2), all of them appear to be in the expected sense and with the expected order of magnitude. Such agreement is remarkable given the simplicity of the Van der Laan model and the limitation of our data.

In order to assess the robustness of our finding, we performed a sensitivity analysis of how interpolated sampling affects the results. As seen in Fig. A.3, the derived lags always reach a constant level after a sufficiently large number of interpolated points. Computing the rms dispersion of the latest 1000 points provides values of ∼1 s comparable to the uncertainty estimates derived with Eq. (3). Figure A.3 also shows that, even with coarse interpolation, the V vs. I_c time lag still remains significant although at a lower level. The V vs. I_c time lag amounts to 86 ± 16 s for $N = 10$ interpolated sampling points. The other filter combinations, V vs. R_c and R vs. I_c, which are closer in wavelength, remain consistent with zero both amounting to 22 ± 16 s.

Moreover, to further ensure the confidence on the lag estimates with interpolated light curves, we conducted a series of simulations by cross-correlating the observed light curves with themselves after introducing different artificial time lags (see Table A.3). Our procedure was able to confidently recover these time lags, within a few seconds, but always with a systematic negative bias that results as an intrinsic effect of the interpolation method used. In our case this is not expected to introduce a severe effect because of the lack of skewness in the time sampling distribution (Rehfeld et al. 2011). Therefore, the measured lag values quoted above should be actually interpreted as lower limits. These two consistency checks reinforce our confidence in the lag detection provided that interpolation is actually a good approximation.

Another test that could be performed is the dependence of the maximum flux densities $S_{m,\lambda}$ as a function of wavelength. Following van der Laan (1966), the expected dependence is:

$$S_{m,\lambda} = S_{m,\lambda_0}[\lambda/\lambda_0]^{-\frac{7p+3}{4p+6}}, \tag{4}$$

considering the same isolated flare as above, and removing the pedestal flux density with a simple linear fit, we estimate the V-band maximum as $S_{m,V} \simeq 1480$ mJy. For $p = 1$, one would then predict $S_{m,R_c} \simeq 1260$ mJy and $S_{m,I_c} \simeq 1010$ mJy. Our R_c and I_c light curves in Fig. 4 were not well sampled to appropriately catch their maxima. With the pedestal flux density removed they provide $S_{m,R_c} \gtrsim 1020$ mJy and $S_{m,V} \gtrsim 650$ mJy, respectively. While the expected values are not exactly reproduced, the results are still compatible.

All together, we consider that this finding is supportive of our tentative interpretation of the optical flares as due to non-thermal plasmon ejection events. Similar flares in the prototypical case of GRS 1915+105 could not be observed in the optical because of the higher interstellar extinction.

In addition, the CCFs in Fig. A.1 display clear secondary maxima corresponding to time lags of ∼1500 s. This agrees with the idea, already expressed before, that the optical light curve of V404 Cygni in outburst during our observation consists of the superposition of flares that appear every half hour on average. Flaring behaviour with a similar timescale is also present in optical light curves reported by other observers just before and after our UJT observations (Scarpaci & Maitra 2015; Scarpaci et al. 2015).

The energy involved in each ejection event can also be derived based on simple equipartition arguments using the Pacholczyk (1970) formulation. Looking at Fig. 4, the flare incremental flux density with respect to the pedestal value is in the range ∼0.5–1.0 Jy, and this occurs typically $\sim 10^3$ s after the estimated onset of the flares. Such flux density increments are comparable to the 1.4 GHz emission levels reported near the time of our observations within a factor of a few. This renders the possibility of a nearly flat synchrotron component from radio to optical wavelengths conceivable. Assuming an expansion velocity of $\sim 0.5c$, the plasmon size at the time of maximum would be $\sim 1.5 \times 10^{13}$ cm. This is equivalent to 0.4 milliarcsec at the V404 Cygni distance and consistent with previous size upper limits. Using this dimension, the radio/optical flux densities quoted before, and assuming relativistic electrons with Lorentz factor $\gamma \leq 10^4$, the total energy content is estimated to be 2×10^{40} erg, with a magnetic field of 12 G. The source brightness temperature does not exceed a few 10^{12} K. Under all such assumptions, the corresponding non-thermal luminosity, from the radio to optical domain, amounts to 2.2×10^{36} erg s^{-1}, which implies a synchrotron life-time of about 2 h for individual flaring events. This is only four times their observed recurrence interval, thus flare superposition should become negligible after a few flaring events. Finally, the plasmon mass involved in the ejection is found to be $\sim 2 \times 10^{20}$ g provided that there is one proton per relativistic electron. These numbers do not differ by more than one order of magnitude when compared with the reference case of GRS 1915+105.

4. Conclusions

We have reported new optical photometric data for the LMXB V404 Cygni during its 2015 June outburst obtained with a small educational telescope. The time interval covered by our observations complements and contributes to the multi-wavelength campaign carried out as a world-wide effort by many observers. From the analysis of our data alone, some interesting findings can already be advanced and we summarize them as follows.

The UJT optical light curves consisted of consecutive and partially overlapping flaring events, appearing about every half hour and with very large amplitudes (∼1 mag). Timescales of variability as short as 10 min could be clearly detected both in brightness and colour. The optical variability observed appears to display a correlation pattern in the colour-colour plane, whose interpretation will deserve future theoretical work.

The de-reddened optical continuum had an average positive spectral index close the +2 value. Thus, for most of the time the observed photometric bands (VR_cI_c) were mainly sampling the Rayleigh Jeans part of the accretion disk spectrum. The V404 Cygni flares, superposed on this continuum, are tentatively interpreted as non-thermal flaring events. With all caution, we suggest that the flares are due to relativistic plasmons ejected following successive replenishing and emptying episodes of the inner accretion disk. The fact that non-thermal, synchrotron emission appears to contribute to optical wavelengths renders V404 Cygni a very interesting system to better study the energetics of black hole LMXBs.

From a CCF analysis, we have found a systematic time lag between the UJT optical light curves acquired with the different filters during our observations. These lags are such that emission at shorter wavelengths precedes emission at longer wavelengths by ∼1 min. This finding was most evident when light curves were resampled and evenly interpolated, which we believe is a reasonable approach when dealing with nearly evenly spaced data. This delay is in qualitative agreement with a simple Van der Laan model for the expansion of a synchrotron emitting plasmon, and the relative amplitude of flare maxima is also consistent. An estimate of the plasmon physical parameters required for the non-thermal spectrum to extend from radio to optical wavelengths appears to be similar to other well-known systems, such as GRS 1915+105.

Acknowledgements. This work was supported by grant AYA2013-47447-C3-3-P from the Spanish Ministerio de Economía y Competitividad (MINECO), and by the Consejería de Economía, Innovación, Ciencia y Empleo of Junta de Andalucía under research group FQM-322, as well as FEDER funds.

References

Barthelmy, S. D., Krimm, H. A., Marshall, F. E., & Siegel, M. H. 2015, GCN Circ., 17929, 1
Bessell, M. S. 1979, PASP, 91, 589
Casares, J., Charles, P. A., & Naylor, T. 1992, Nature, 355, 614
Casares, J., Charles, P. A., Naylor, T., & Pavlenko, E. P. 1993, MNRAS, 265, 834
Cousins, A. W. J. 1974a, MNRAS, 166, 711
Cousins, A. W. J. 1974b, Mon. Notes Astron. Soc. South Afr., 33, 149
Edelson, R. A., & Krolik, J. H. 1988, ApJ, 333, 646
Hardy, L., Littlefair, S., Dhillon, V., Butterley, T., & Wilson, R. 2015, ATel, 7681, 1
Hynes, R. I., Robinson, E. L., & Morales, J. 2015, ATel, 7677, 1
Johnson, H. L., & Morgan, W. W. 1953, ApJ, 117, 313
Kitamoto, S., Tsunemi, H., Miyamoto, S., Yamashita, K., & Mizobuchi, S. 1989, Nature, 342, 518
Mathis, J. S. 2000, in Allen's astrophysical quantities, ed. A. N. Cox, Chap. 21, 523
Miller-Jones, J. C. A., Jonker, P. G., Dhawan, V., et al. 2009, ApJ, 706, L230
Mirabel, I. F., Dhawan, V., Chaty, S., et al. 1998, A&A, 330, L9
Mooley, K., Fender, R., Anderson, G., et al. 2015, ATel, 7658, 1
Negoro, H., Matsumitsu, T., Mihara, T., et al. 2015, ATel, 7646, 1
Pacholczyk, A. G. 1970, Radio Astrophysics: Nonthermal Processes in Galactic and Extragalactic Sources, Astronomy and Astrophysics Series (W. H. Freeman)
Rehfeld, K., Marwan, N., Heitzig, J., & Kurths, J. 2011, Nonlin. Proc. Geophys., 18, 389
Reynolds, M. T., Reis, R. C., Miller, J. M., Cackett, E. M., & Degenaar, N. 2014, MNRAS, 441, 3656
Rodriguez, J., Cadolle Bel, M., Alfonso-Garzón, J., et al. 2015, A&A, 581, L9
Scarpaci, J., & Maitra, D. 2015, ATel, 7721, 1
Scarpaci, J., Maitra, D., Hynes, R., & Markoff, S. 2015, ATel, 7737, 1
Tsubono, K., Aoki, T., Asuma, K., et al. 2015, ATel, 7733, 1
van der Laan, H. 1966, Nature, 211, 1131
Wagner, R. M., Kreidl, T. J., Howell, S. B., & Starrfield, S. G. 1992, ApJ, 401, L97
White, R. J., & Peterson, B. M. 1994, PASP, 106, 879
Wiersema, K. 2015, ATel, 7688, 1

Appendix A: Additional material

Table A.1. AAVSO comparison stars used in this work.

AAVSO Id.	RA(J2000.0) (hms)	Dec(J2000.0) (dms)	B (mag)	V (mag)	R_c (mag)	I_c (mag)
125	20:23:56.47	+33:48:16.9	12.976 0.019	12.497 0.014	12.204 0.018	11.926 0.018
128	20:24:07.24	+33:50:52.2	13.499 0.017	12.815 0.014	12.384 0.018	11.967 0.018
132	20:24:08.89	+33:54:38.6	13.879 0.018	13.164 0.012	12.712 0.016	12.284 0.016
134	20:23:53.43	+33:52:24.6	14.467 0.017	13.361 0.015	12.737 0.019	12.203 0.019

Table A.2. Optical photometry of V404 Cygni wiht the UJT telescope.

MJD*	V-band (mag)	MJD*	R_c-band (mag)	MJD*	I_c-band (mag)
57 199.91379	12.842 ± 0.012	57 199.91456	11.488 ± 0.007	57 199.91532	10.468 ± 0.009
57 199.91610	12.825 ± 0.013	57 199.91686	11.476 ± 0.008	57 199.91763	10.299 ± 0.010
57 199.91840	12.547 ± 0.011	57 199.91916	11.258 ± 0.008	57 199.91993	10.231 ± 0.012
57 199.92070	12.613 ± 0.013	57 199.92146	11.325 ± 0.007	57 199.92223	10.222 ± 0.009
57 199.92478	12.797 ± 0.014	57 199.92554	11.476 ± 0.006	57 199.92631	10.401 ± 0.009
57 199.92708	12.731 ± 0.015	57 199.92785	11.364 ± 0.006	57 199.92861	10.309 ± 0.010
57 199.92938	12.707 ± 0.013	57 199.93015	11.354 ± 0.006	57 199.93091	10.280 ± 0.009
57 199.93169	12.688 ± 0.012	57 199.93245	11.402 ± 0.010	57 199.93322	10.438 ± 0.010
57 199.93399	12.912 ± 0.012	57 199.93476	11.589 ± 0.008	57 199.93552	10.568 ± 0.012
57 199.93629	12.948 ± 0.016	57 199.93706	11.640 ± 0.006	57 199.93782	10.598 ± 0.011
57 199.93860	13.013 ± 0.018	57 199.93936	11.655 ± 0.007	57 199.94013	10.639 ± 0.010
57 199.94090	13.095 ± 0.013	57 199.94167	11.739 ± 0.009	57 199.94243	10.808 ± 0.009
57 199.94320	13.241 ± 0.016	57 199.94397	11.814 ± 0.008	57 199.94473	10.779 ± 0.009
57 199.94551	13.241 ± 0.017	57 199.94627	11.881 ± 0.008	57 199.94704	10.847 ± 0.011
57 199.94781	13.455 ± 0.014	57 199.94858	12.172 ± 0.010	57 199.94934	11.194 ± 0.010
57 199.95012	13.539 ± 0.018	57 199.95088	11.944 ± 0.008	57 199.95165	10.901 ± 0.012
57 199.95252	13.401 ± 0.018	57 199.95328	12.031 ± 0.007	57 199.95405	11.060 ± 0.012
57 199.95482	13.480 ± 0.018	57 199.95559	11.980 ± 0.009	57 199.95635	10.966 ± 0.009
57 199.957 12	13.391 ± 0.013	57 199.95789	11.900 ± 0.008	57 199.95866	10.841 ± 0.010
57 199.95943	13.194 ± 0.014	57 199.96019	11.794 ± 0.007	57 199.96096	10.708 ± 0.011
57 199.96173	12.977 ± 0.011	57 199.96250	11.584 ± 0.008	57 199.96326	10.517 ± 0.010
57 199.96404	12.920 ± 0.011	57 199.96480	11.724 ± 0.007	57 199.96557	10.796 ± 0.010
57 199.96634	13.333 ± 0.013	57 199.96711	12.024 ± 0.006	57 199.96787	11.065 ± 0.009
57 199.96865	13.631 ± 0.016	57 199.96941	12.102 ± 0.006	57 199.97018	11.086 ± 0.011
57 199.97095	13.608 ± 0.020	57 199.97172	12.271 ± 0.007	57 199.97248	11.285 ± 0.015
57 199.97326	13.677 ± 0.021	57 199.97402	12.126 ± 0.007	57 199.97479	11.068 ± 0.012
57 199.97556	13.444 ± 0.014	57 199.97632	12.157 ± 0.007	57 199.97709	11.163 ± 0.011
57 199.97786	13.500 ± 0.016	57 199.97863	12.050 ± 0.006	57 199.97939	10.966 ± 0.009
57 199.98017	13.354 ± 0.013	57 199.98093	11.995 ± 0.007	57 199.98170	10.952 ± 0.012
57 199.98247	13.166 ± 0.013	57 199.98324	11.801 ± 0.007	57 199.98400	10.695 ± 0.011
57 199.98478	13.059 ± 0.014	57 199.98554	11.872 ± 0.007	57 199.98631	10.818 ± 0.009
57 199.98708	13.235 ± 0.011	57 199.98785	11.862 ± 0.007	57 199.98861	10.838 ± 0.010
57 199.98938	13.383 ± 0.018	57 199.99015	12.152 ± 0.006	57 199.99091	11.224 ± 0.010
57 199.99169	13.720 ± 0.014	57 199.99245	12.235 ± 0.007	57 199.99322	11.233 ± 0.013
57 199.99399	13.696 ± 0.014	57 199.99476	12.250 ± 0.007	57 199.99552	11.074 ± 0.014
57 199.99629	13.354 ± 0.012	57 199.99706	11.845 ± 0.007	57 199.99782	10.727 ± 0.011
57 200.00593	13.287 ± 0.018	57 200.00669	12.022 ± 0.007	57 200.00746	11.032 ± 0.012
57 200.00823	13.317 ± 0.012	57 200.00900	11.992 ± 0.006	57 200.00976	10.870 ± 0.011
57 200.01054	13.285 ± 0.011	57 200.01130	11.961 ± 0.006	57 200.01207	10.955 ± 0.012
57 200.01284	13.297 ± 0.013	57 200.01361	11.931 ± 0.008	57 200.01437	10.941 ± 0.012
57 200.01514	13.457 ± 0.012	57 200.01591	12.160 ± 0.007	57 200.01667	10.994 ± 0.011
57 200.01745	13.291 ± 0.013	57 200.01821	11.941 ± 0.006	57 200.01898	10.945 ± 0.013
57 200.01975	13.588 ± 0.016	57 200.02052	12.265 ± 0.007	57 200.02128	11.256 ± 0.013
57 200.02205	13.550 ± 0.021	57 200.02282	11.984 ± 0.007	57 200.02358	10.745 ± 0.014
57 200.02435	12.914 ± 0.014	57 200.02512	11.559 ± 0.008	57 200.02588	10.425 ± 0.012
57 200.02665	12.755 ± 0.009	57 200.02742	11.457 ± 0.007	57 200.02818	10.406 ± 0.013
57 200.02896	12.827 ± 0.014	57 200.02972	11.436 ± 0.006	57 200.03049	10.337 ± 0.014
57 200.03126	12.646 ± 0.016	57 200.03203	11.378 ± 0.006	57 200.03279	10.406 ± 0.016
57 200.03357	12.986 ± 0.011	57 200.03433	11.741 ± 0.010	57 200.03510	10.787 ± 0.016
57 200.03587	13.294 ± 0.015	57 200.03663	11.853 ± 0.008	57 200.03740	10.811 ± 0.016
57 200.03817	13.249 ± 0.015	57 200.03894	11.916 ± 0.008	57 200.03970	10.951 ± 0.021

Notes. (*) The Modified Julian Date (MJD) given is heliocentric and corresponds to the mid-exposure time.

Table A.3. Recovered artificial time lags with interpolated sampling CCF for V-band data.

Artificial time lag (s)	Recovered time lag (s)	Artificial time lag	Recovered time lag
0	−0.02	60	52.92
1	−0.02	70	62.85
5	−0.02	80	72.80
10	3.22	90	82.73
20	13.15	100	92.66
30	23.08	110	102.59
40	33.06	120	112.52
50	42.99	1000	971.77

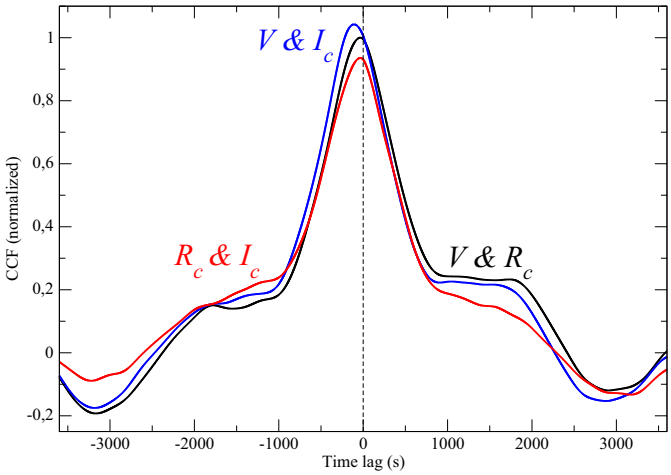

Fig. A.1. CCFs of the optical light curves V vs. R_c (black), V vs. I_c (blue) and R_c vs. I_c (red). The vertical dashed line corresponds to zero time lag. The V vs. R_c CCF is normalized to unity while the other two have been slightly scaled above and below for easier display.

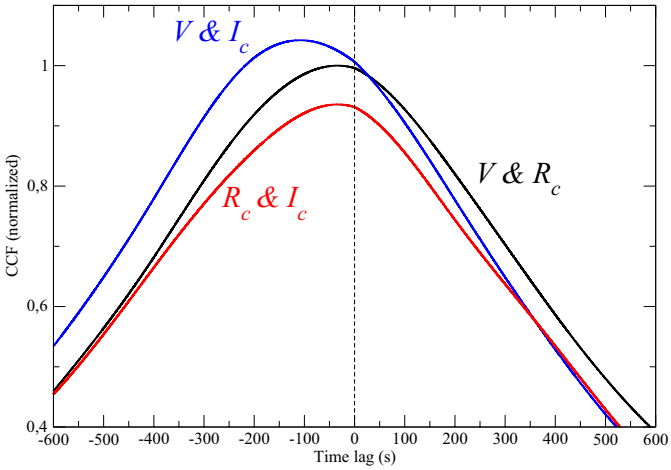

Fig. A.2. Zoomed view of the central maxima of the CCFs where a clear asymmetry is visible. Colours and normalization are as in Fig. A.1.

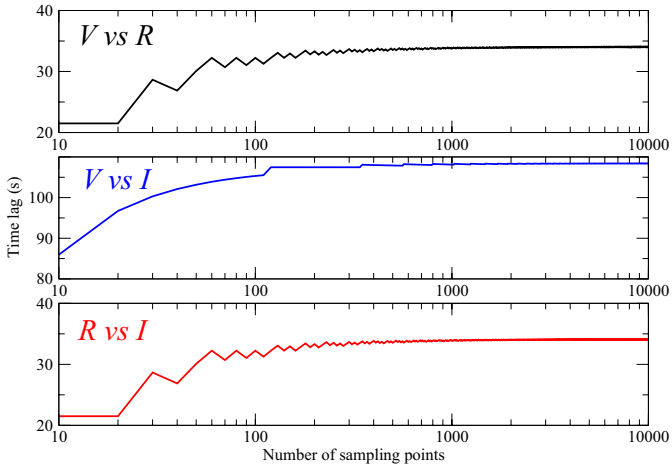

Fig. A.3. Dependence of the derived time lags using the cross-correlation technique on the amount of interpolated sampling of the data. Colours are as in Figs. A.1 and A.2.